The atomic-scale structure of LaCrO3-NaTaO3 solid solution photocatalysts with enhanced electron population

Sudrajat, Hanggara
Zhou, Yizhong
Sasaki, Takuro
Ichikuni, Nobuyuki
Onishi, Hiroshi

(Citation)
Physical Chemistry Chemical Physics,21(9):5148-5157

(Issue Date)
2019-03-07

(Resource Type)
journal article

(Version)
Accepted Manuscript

(URL)
https://hdl.handle.net/20.500.14094/90005830

Journal Name

ARTICLE

Atom-scale structure of $LaCrO_3$-$NaTaO_3$ solid solution photocatalysts with enhanced electron population

Received 00th January 20xx,
Accepted 00th January 20xx

DOI: 10.1039/x0xx00000x

www.rsc.org/

Hanggara Sudrajat,*[a] Yizhong Zhou,[a] Takuro Sasaki,[b] Nobuyuki Ichikuni[b] Hiroshi Onishi[a]

Visible light sensitization of sodium tantalate ($NaTaO_3$), a highly UV-active material, is critical for realizing its practical application in photocatalytic water splitting under solar light. Double doping of half-filled transition metal together with another metal for cationic charge balance is a promising way of sensitizing $NaTaO_3$ to visible light. One fundamental issue is the atom-scale structure of such doubly doped $NaTaO_3$ that has not yet been fully understood. In this study, we doubly doped $NaTaO_3$ with La^{3+} and Cr^{3+} through a solid-state route. The occupation preference of La^{3+} in the doubly doped system was particularly studied by extended X-ray absorption fine structure. We revealed the substitution of La^{3+} for Na^+, and Cr^{3+} for Ta^{5+}, forming a $LaCrO_3$-$NaTaO_3$ solid solution. We then showed that doping $NaTaO_3$ with La^{3+} and Cr^{3+} appreciably increased the population of electrons photoexcited by UV light. Photoactivating the doubly doped $NaTaO_3$ with visible light produced electrons with population comparable to that under UV light. The charge compensation scheme of double doping with La^{3+} and Cr^{3+} is shown here to be a good option for the sensitization of $NaTaO_3$ to visible light.

1. Introduction

Photocatalysis for H_2 evolution through water splitting reaction has sparked tremendous attention over the last two decades.[1-3] For UV-induced photocatalytic water splitting, $NaTaO_3$ has been known to be highly active and possesses excellent stability.[4-7] When $NaTaO_3$ was doped with La^{3+}, it exhibited an apparent quantum yield of water splitting as high as 56% under UV light.[4] Onishi and co-workers then revealed that charge carrier recombination was effectively restricted in La-doped $NaTaO_3$.[8] Despite major breakthrough in photocatalytic water splitting with La-doped $NaTaO_3$, practical application of this photocatalyst seems to be rather limited, because it is unable to absorb visible light which occupies up to 46% of the total solar energy. Therefore, sensitizing $NaTaO_3$ to visible light is crucial to deal with such a bottleneck that nowadays becomes the most pressing issue with photocatalysis.

Doping half-filled transition metal together with La^{3+} is a promising way of sensitizing $NaTaO_3$ without need for oxygen vacancies as cationic charge is balanced. Recently, $NaTaO_3$ doubly doped with La^{3+} and Cr^{3+} and loaded with Pt co-catalyst was reported to show promising photocatalytic activity for water splitting in the presence of methanol as the sacrificial reagent.[9] The rate of H_2 evolution reached 4.5 µmol h^{-1} with an apparent quantum yield of 0.5%. In another report with the same photocatalyst, a H_2 evolution rate of 4 µmol h^{-1} was documented.[10] Despite progresses witnessed, fundamental insights into the structure of the mentioned photocatalyst, especially at the atomic scale, have not yet been available. Limited understanding of the atom-scale structure makes finding out the key factors behind the improved photocatalytic activity become considerably challenging. Then, without knowing why the photocatalytic activity of $NaTaO_3$ is improved upon doping with La^{3+} and Cr^{3+}, research on this promising photocatalyst material is difficult to be properly directed.

The objective of this study is to reveal the atom-scale structure of $NaTaO_3$ doubly doped with La^{3+} and Cr^{3+}. The critical issue is the occupation preference of La^{3+} in the doubly doped system. Here, we hypothesize that La^{3+} replaces Na^+, while Cr^{3+} replaces Ta^{5+}, forming a $LaCrO_3$-$NaTaO_3$ solid solution. This hypothesis comes from the fact that the ionic radii of the dopants are similar to those of the replaced cations. We also notice that both $NaTaO_3$ and $LaCrO_3$ have the same crystal structure of orthorhombic at room temperature. In this circumstance, substantial lattice strain should not be produced, and the formation of a $LaCrO_3$-$NaTaO_3$ solid solution is therefore favorable. In fact, where La^{3+} and Cr^{3+} are situated in the lattice of the host $NaTaO_3$ has been under debate. Yi and Ye proposed occupation of the Na site by La^{3+}, and the Ta site by Cr^{3+}.[9] In contrast, Yang and co-workers proposed simultaneous occupation of the Na site and the Ta site by La^{3+}.[10] Either the former or the latter proposal is offered based on the continuous expansion of lattice volume observed upon double doping. Indeed, thus far, the occupation preference of La^{3+} remains unclear. Encouraged by this situation, in this study, we used extended X-ray absorption fine structure (EXAFS) to clarify where La^{3+} is incorporated in the doubly doped $NaTaO_3$. By using EXAFS, determining the local environment around the

[a] Department of Chemistry, Graduate School of Science, Kobe University, Kobe 657-8501, Japan
[b] Department of Applied Chemistry and Biotechnology, Graduate School of Engineering, Chiba University, Chiba 263-8522, Japan.
† Footnotes relating to the title and/or authors should appear here.
Electronic Supplementary Information (ESI) available: [details of any supplementary information available should be included here]. See DOI: 10.1039/x0xx00000x

guest La^{3+} being doped in the host $NaTaO_3$ is possible. We expect that our understanding of this photocatalyst system will be improved and a proper research direction can ultimately be procured.

2. Experimental section

2.1 Photocatalyst preparation

Here, La^{3+} and Cr^{3+} were doped into $NaTaO_3$ (NTO) through the two-step solid-state route,[4] as illustrated in Figure S1 (Supporting Information). In a typical protocol, a mixture of Na_2CO_3 (99.8%, Kanto), Ta_2O_5 (99.99%, Rare Metallic), La_2O_3 (99.99%, Wako), and Cr_2O_3 (99.9%, Wako) was ground into a very fine powder at room temperature for 30 min in an agate mortar followed by calcination in an alumina crucible at 1173 K for 1 h. Prior to subsequent calcination at 1423 K for 10 h, grinding of the calcined powder was carried out for 30 min. The Na/Ta molar ratio in the mixture was fixed to 1.05. Meanwhile, the La/Ta and Cr/Ta molar ratios were tuned to 0, 1, 2, 4, 8, 20, 50, and 75%. Unreacted Na^+ left in the calcined product was washed out with water. The final products were denoted as LaCr-NTO (*x*+*x* mol%), where *x* represents the concentration of La^{3+}, or Cr^{3+}, relative to that of Ta^{5+}.

2.2 Photocatalyst characterization

The formation of $NaTaO_3$ was confirmed with an X-ray diffractometer (Rigaku, SmartLab). The actual concentrations of La^{3+} and Cr^{3+} in the host $NaTaO_3$ were quantified relative to that of Ta^{5+} using an energy dispersive X-ray fluorescence (EDX) spectrometer (Shimadzu, EDX-720). The shape of the photocatalyst particles was inspected with a scanning electron microscope (Hitachi High-Technologies, S-4800). The light absorption of the photocatalyst was measured with ultraviolet-visible diffuse reflection spectroscopy (UV-Vis DRS) using a spectrometer (Jasco, V-570) equipped with an integration sphere. Quantification of the actual concentrations of La^{3+} and Cr^{3+} on the photocatalyst surface was performed with X-ray photoelectron spectroscopy (XPS) using a spectrometer (Ulvac-Phi, PHI X-tool) with an Al Kα X-ray source. A Raman spectrometer (Jasco, NRS-7100) was employed for observing breathing vibration in $NaTaO_3$, if any. Excitation wavelength of 532 nm and excitation power of 60 mW were adopted in the Raman measurement. Light-induced IR absorption spectra were measured using a Fourier transform spectrometer (Jasco, FT/IR610). For the IR measurement, each sample was first suspended in water with a weight concentration of 3 g L^{-1}. Subsequently, 0.5 mL of the suspension was transferred to a CaF_2 plate with a thickness of 1 mm and then heated at 573 K for 3 h to remove organic contaminants attached on the photocatalyst film. The CaF_2 plate covered by the photocatalyst sample was placed in a vacuum of 10 Pa. Absorbance spectra under UV light, or visible light, were then recorded. A 200-Watt mercury-xenon lamp (San-ei Electric, UVS-204S) was used as the UV light source. Light intensity at wavelengths of shorter than 380 nm was 30 mW cm^{-2}. Meanwhile, visible light was provided by a 300-Watt xenon lamp (Asahi Spectra, MAX-302). Light intensity at wavelengths of 385-740 nm was 34 mW cm^{-2}. Here, the IR measurement was intended to simulate the number of electrons available in water splitting reaction.

2.3 X-ray absorption measurement

Absorption spectra at the La *K*-edge of La_2O_3, $LaCrO_3$, LaCr-NTO (20+20 mol%), and LaCr-NTO (8+8 mol%) were recorded in the transmission mode at the AR-NW10A of Photon Factory, Tsukuba, Japan. Meanwhile, those of LaCr-NTO (4+4 mol%), LaCr-NTO (2+2 mol%), and LaCr-NTO (1+1 mol%) were recorded in the fluorescence mode using a 19-element solid-state detector at the same beamline. The obtained EXAFS data were analyzed by ATHENA and ARTEMIS programs with the programmer's interface of IFEFFIT.[11]

3. Results & discussions

3.1 Crystallographic phase

In this research, doping of $NaTaO_3$ with La^{3+}, Cr^{3+}, or La^{3+} and Cr^{3+} was done with the two-step solid-state route.[4] Solid-state route is frequently used for preparing perovskite-structured $NaTaO_3$ due to its simplicity and robustness. Here, the formation of $NaTaO_3$ was confirmed with XRD. Figure 1 shows the XRD patterns of pristine $NaTaO_3$ and singly doped $NaTaO_3$. The observed diffraction angles and peak intensities were identical to those reported earlier.[9,10] All the patterns were well assigned to the orthorhombic structure. Single phase of perovskite-structured $NaTaO_3$ was always obtained for all the singly doped $NaTaO_3$. Impurity phases involving chromium oxides or lanthanum oxides were not observed above the detection limit of the employed XRD. In order to make clearer the main peak position, the diffractograms around the (002) peak and the (112) peak were magnified in Figure 1b and Figure 1c, respectively. No peak shifts were observed in Cr-NTO (2 mol%). Meanwhile, in La-NTO (2 mol%), the peaks were slightly shifted to lower angles and broadened, probably due to the lattice expansion as a result of partial occupation of the Ta site by the much larger La^{3+}. Kato and co-workers, nevertheless, assigned the observed low-angle shifts upon doping of $NaTaO_3$ with La^{3+} to be due to the Na site occupation by La^{3+}.[4] In their scheme, the Ta site is not occupied by La^{3+}. This assignment is based on the fact that the diffraction pattern of $La_{0.33}TaO_3$, which has the Na site occupation factor of 0.3, is very similar to that of La-$NaTaO_3$.[12] In addition, as compared to those of $NaTaO_3$, the diffraction peaks of $La_{0.33}TaO_3$ appeared at lower angles.

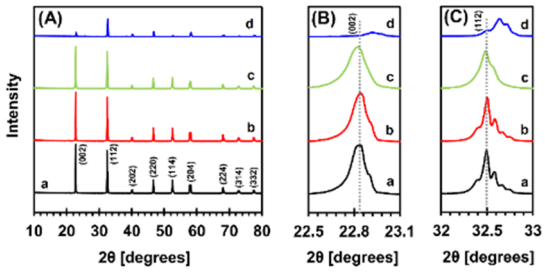

Figure 1. XRD patterns of a: NTO, b: Cr-NTO (2 mol%), c: La-NTO (2 mol%), and d: $LaCrO_3$ in the range of (A) 10-80°, (B) 22.5-23.1°, and (C) 32-33°.

In the present study, the XRD pattern of $LaCrO_3$ was also checked for comparison, and confirmed to possess orthorhombic symmetry.[13] The diffraction peaks of $LaCrO_3$ were observed at higher angles than those of the doped $NaTaO_3$ due to a lower lattice volume of $LaCrO_3$.

Figure 2 shows the XRD patterns of all the doubly doped $NaTaO_3$. The XRD patterns of pristine $NaTaO_3$ and $LaCrO_3$ were also shown and stacked vertically for easy comparison. With increasing the dopant concentration, the diffraction peaks gradually shifted to lower angles and continuously broadened. The observed peak broadening indicated the decrease of particle size upon doping. Moreover, small peak shifts were generally seen after doping $NaTaO_3$. Such small peak shifts indicated small lattice changes. There was not much distortion or strain in the host lattice due to the substitution of dopants. The low-angle shifts of the diffraction peaks after simultaneous incorporation of La^{3+} and Cr^{3+} into $NaTaO_3$ were also reported by other groups.[9,10,14] Their results are consistent with our observations. Yang and co-workers suggested partial occupation of the Ta site by La^{3+} to be the reason behind such low-angle shifted diffraction peaks.[10] In this scenario, La^{3+} simultaneously substituted for the Na site and the Ta site, while Cr^{3+} substituted for the Ta site. Therefore, lattice expansion then occurred. Their proposed scenario seems reasonable. The ionic radius of 12-coordinated La^{3+} (1.36 Å)[4] is smaller than that of Na^{+} (1.39 Å)[4], and the ionic radius of 6-coordinated Cr^{3+} (0.61 Å)[10] is also smaller than that of Ta^{5+} (0.64 Å)[4]. Thus, the lattice volume of $LaCrO_3$ (234.8 $Å^3$)[15] is smaller than that of $NaTaO_3$ (235.5 $Å^3$)[16] at room temperature. If substitutions of the Na site by La^{3+} and the Ta site by Cr^{3+} take place, it would lead to a lattice shrinkage. However, they observed a lattice expansion instead, suggesting that not only Cr^{3+} but also La^{3+} should have occupied the Ta sites. On the other hand, Yi and Ye suggested exclusive occupation of the Na site by La^{3+}, and the Ta site by Cr^{3+}, forming a $LaCrO_3$-$NaTaO_3$ solid solution despite continuous increase of lattice volume upon increasing the dopant concentration.[9] Recently, LaCr-NTO photocatalysts prepared by spray pyrolysis also showed continuous low-angle shift due to the increased lattice constant, and hence lattice volume, when the dopant concentration was systematically increased.[14] Replacement of Na^{+} by La^{3+}, and Ta^{5+} by Cr^{3+}, was also proposed in that study. As witnessed here, two opposing scenarios for interpreting the low-angle shift of diffraction peak in LaCr-NTO were offered.[9,10,14] Given the unsettled conclusion, the complexity of the replacement process and thus the resulting structure were clearly demonstrated here.

One may propose an alternative interpretation of shifted diffraction peaks based on the popular scenario of anion or cation vacancies. Anion vacancies, e.g. oxygen vacancies, are believed to result in an expanded lattice in perovskite systems, while cation vacancies can generally lead the opposite effect.[17] Charge compensation of doped cations was present in the here system of LaCr-NTO, nevertheless. Cr^{3+} was stably doped in NTO by the presence of La^{3+}. Formation of Cr cations with higher oxidation states or oxygen vacancies is therefore not needed. Cation vacancies, e.g. Na vacancies, can also be ruled out here, because an excess amount of Na (5 mol%) was added in the mixture of reactants to compensate for volatilization of Na during high-temperature calcination that may induce Na vacancies.

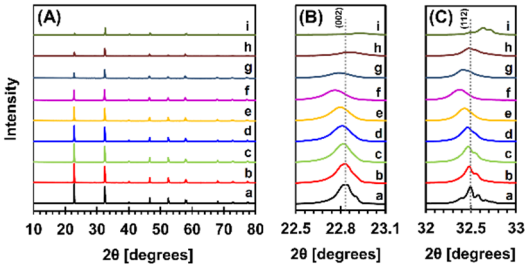

Figure 2. XRD patterns of a: NTO, b: LaCr-NTO (1+1 mol%), c: LaCr-NTO (2+2 mol%), d: LaCr-NTO (4+4 mol%), e: LaCr-NTO (8+8 mol%), f: LaCr-NTO (20+20 mol%), g: LaCr-NTO (50+50 mol%), h: LaCr-NTO (75+75 mol%), and i: $LaCrO_3$ in the range of (A) 10-80°, (B) 22.5-23.1°, and (C) 32-33°.

To get a better understanding on the examined structure, we prepared doubly doped samples with considerably high dopant concentrations: LaCr-NTO (50+50 mol%) and LaCr-NTO (75+75 mol%). The diffraction peaks of those two photocatalysts shifted to higher angles relative to those of LaCr-NTO (20+20 mol%) and approached those of $LaCrO_3$ (Figure 2). Although the reasons for the peak shift to switch from low-angle to high-angle at a dopant concentration of 20+20 mol% are unknown at present, we tended to believe that the observed continuous peak shifts are indicative of the formation of a $LaCrO_3$-$NaTaO_3$ solid solution. This indication came from the fact that the diffraction peaks ultimately shifted to those of $LaCrO_3$. In addition, the intensity ratio of the (002) peak to the (112) peak of the LaCr-NTO samples became closer to that of $LaCrO_3$ when the dopant concentration was gradually increased.

3.2 Chemical composition

To gain insight into the dopant composition in the host $NaTaO_3$, we plotted the initial dopant concentration with respect to the actual dopant concentration determined by EDX. As shown in Figure 3, straight lines were well fitted to the observed concentrations. Figure 4 presents the actual La/Cr molar ratio as a function of the initial dopant concentration. One-to-one ratio of the La^{3+} and Cr^{3+} incorporation in the bulk was indicated. The substitution scheme of La^{3+} for Na^{+}, and Cr^{3+} for Ta^{5+}, forming a $LaCrO_3$-$NaTaO_3$ solid solution, was therefore supported by this finding.

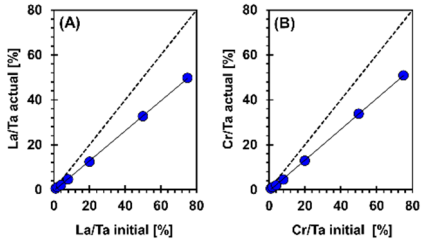

Figure 3. Actual dopant concentration determined by EDX as a function of initial dopant concentration introduced in the preparation of LaCr-NTO for (A) La^{3+} and (B) Cr^{3+} dopants. The dashed line represents the relationship with a slope of unity.

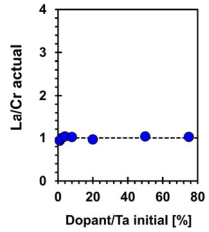

Figure 4. Actual La/Cr molar ratio determined by EDX as a function of initial dopant concentration. The dashed line represents a La/Cr molar ratio of 1 initially adopted in the preparation of LaCr-NTO.

3.3 Raman scattering

To seek for further hints on the occupation preference of the dopants, particularly La^{3+}, we then employed Raman spectroscopy. Figure 5 shows the Raman spectra of $NaTaO_3$ and all the doubly doped $NaTaO_3$. A main peak at about 620 cm^{-1} was produced in all the photocatalyst samples. This characteristic peak was previously reported[18] and was assigned to the lattice vibrations of NaO_{12} cuboctahedron in $NaTaO_3$. The Raman spectrum of $LaCrO_3$ was not shown here. This was because no Raman peaks were observable in $LaCrO_3$ since the intensity of Raman scattering remained much weaker than that of fluorescence emission even when excitation wavelength of 1064 nm was used.

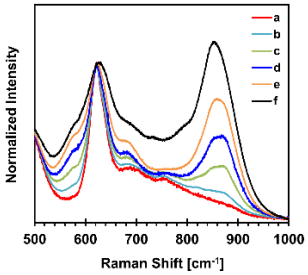

Figure 5. Raman spectra of a: NTO, b: LaCr-NTO (1+1 mol%), c: LaCr-NTO (2+2 mol%), d: LaCr-NTO (4+4 mol%), e: LaCr-NTO (8+8 mol%), and f: LaCr-NTO (20+20 mol%).

Simultaneously incorporating La^{3+} and Cr^{3+} into $NaTaO_3$ produced a pronounced, well-separated peak at 860 cm^{-1}. We assigned the peak appearing at 860 cm^{-1} to be due to the breaking down of the symmetry restriction for the breathing vibrations of TaO_6 octahedron in $NaTaO_3$. Our previous study on Sr-doped $NaTaO_3$ (Sr-NTO) suggested that the occupation of the Ta site by Sr^{2+} was behind the appearance of the 860 cm^{-1} peak.[19] In analogy to Sr-NTO, the Ta sites of the LaCr-NTO samples must have been occupied by the dopants. As shown in Figure S2, the 860 cm^{-1} band remained present in LaCr-NTO (50+50 mol%) and LaCr-NTO (75+75 mol%). Hence, the existence of the 860 cm^{-1} band is indeed an evidence of the Ta site occupation in LaCr-NTO.

Further, relative intensity of the 860 cm^{-1} peak was plotted as a function of the actual dopant concentration determined by EDX in Figure 6. With increasing the dopant concentration, the relative intensity of the 860 cm^{-1} peak systematically increased. The appearance of the 860 cm^{-1} peak was thus evidently caused by the dopants which must have been incorporated in the lattice. It was impossible with Raman technique, however, to know precisely which dopant(s) has occupied the Ta sites: Cr^{3+}, La^{3+}, or Cr^{3+} and La^{3+}. Back to our main issue: that is the occupation preference of La^{3+} in the doubly doped $NaTaO_3$, Raman technique was unfortunately unable to unambiguously clarify whether La^{3+} has also resided in the Ta site. In spite of its inability to address the raised issue, the Raman technique remains important in our case to exclude a physical mixture of $LaCrO_3$ and $NaTaO_3$. A merely physical mixture of $LaCrO_3$ and $NaTaO_3$ instead of a $LaCrO_3$-$NaTaO_3$ solid solution is highly unlikely to exist in our system. This is primarily because such a physical mixture cannot generate the 860 cm^{-1} Raman peak since the Ta^{5+} in $NaTaO_3$ is not replaced.

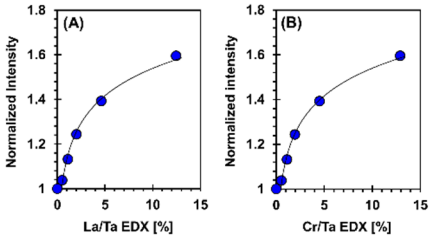

Figure 6. Intensity of Raman peak of LaCr-NTO samples at 860 cm^{-1} relative to that of NTO as a function of dopant concentration for (A) La^{3+} and (B) Cr^{3+} dopants.

3.4 Light absorption

Figure 7 shows the diffuse reflectance (DR) spectra of all the photocatalyst samples. Upon doping of $NaTaO_3$ with Cr^{3+} and La^{3+}, an absorption tail up to 430 nm appeared while the absorption edge remained relatively unchanged. This was an indication of the formation of a new localized state within the band gap. The electron transitions from the Cr-induced state to CB plausibly absorbed light at wavelengths of 320 to 430 nm. The double doping also produced two additional absorption peaks which emerged at about 460 and 640 nm. These two characteristic peaks may be caused by the electron transition within the *d* orbitals of Cr^{3+},[9] which was partially filled. Here, continuous extension of light absorption with the increase of dopant concentration was witnessed. The intensity of the spectra gradually approached that of $LaCrO_3$ when the dopant concentration was increased. The shape of the extended absorbance in the doubly doped $NaTaO_3$ was also essentially similar to that in $LaCrO_3$. Three features of absorption peaks were observed, indicating the presence of $LaCrO_3$ solved in the structure,[9] and thus the formation of a $LaCrO_3$-$NaTaO_3$ solid solution. When physically observing the photocatalysis sample, we noticed that its color gradually changed from a white of $NaTaO_3$ to a pale green of LaCr-NTO, and finally to a dark green of $LaCrO_3$ (Figure S3).

One may suggest a physical mixture of La-NTO and Cr-NTO to be formed in the photocatalyst samples. Such a physical mixture was implausible to exist, nonetheless. As evidenced in Figure S4a for instance, the diffuse reflectance spectrum of a physical mixture of 50 wt% La-NTO (4 mol%) and 50 wt% Cr-NTO (4 mol%) after the absorption edge did not resemble that of LaCr-NTO (4+4 mol%). There was an intermediate absorption peaked around 380 nm in the physical mixture. Also, the Raman spectrum of the physical mixture

was not identical to that of LaCr-NTO (4+4 mol%), as seen in Figure S4b. The intensity of the 860 cm^{-1} peak was much lower in the physical mixture.

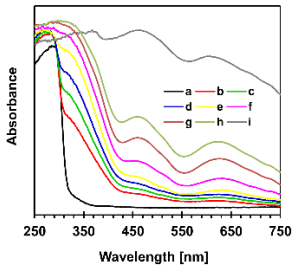

Figure 7. DR spectra of a: NTO, b: LaCr-NTO (1+1 mol%), c: LaCr-NTO (2+2 mol%), d: LaCr-NTO (4+4 mol%), e: LaCr-NTO (8+8 mol%), f: LaCr-NTO (20+20 mol%), g: LaCr-NTO (50+50 mol%), h: LaCr-NTO (75+75 mol%), and i: $LaCrO_3$.

3.5 Particle shape

Figure 8 shows the SEM images of some selected samples. Pristine NTO was composed of spherical cube particles with an average size of about 3 µm. Simultaneously incorporating La^{3+} and Cr^{3+} into NTO resulted in decreased particle size and altered particle shape. The shape of the particles became more cubic. Increasing the dopant concentration led to further decrease of the particle size. As observed in Figure 8, the particle shape remained relatively the same, yet the particle size was quite sensitive to the dopant concentration. Surface reconstruction into terraces and steps was not observed, indicating the absence of lattice mismatch. Here, La^{3+} and Cr^{3+} were well received by $NaTaO_3$. Considering the similarity between the ionic radii of the impurities and those of the replaced cations, tensile stress in the host lattice should have been small here. Quite the reverse, an earlier report indicated surface reconstruction upon single doping of $NaTaO_3$ with La^{3+},[4] as was also observed in our NTO sample singly doped with 2 mol% of La^{3+} (Figure S5). While it was somewhat premature to speculate on the detailed mechanism of the dopant incorporation, it was conclusive that the incorporation mode of La^{3+} in the doubly doped NTO involving Cr^{3+} was different from that in the singly doped La-NTO without Cr^{3+}. In the doubly doped LaCr-NTO, La^{3+} exclusively occupied the Na site, while Cr^{3+} occupied the Ta site. In La-NTO, La^{3+} simultaneously occupied both the Na site and the Ta site. The result in the latter case was an expanded lattice that eventually induced lattice mismatch, and hence surface reconstruction.

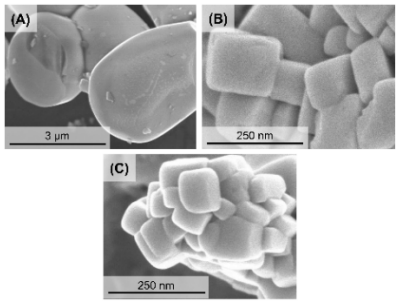

Figure 8. SEM images of (A) NTO, (B) LaCr-NTO (2+2 mol%), and (C) LaCr-NTO (20+20 mol%).

3.6 X-ray absorption spectroscopy

The details of the local structure around La^{3+} in the doubly doped NTO were investigated by EXAFS. Here, attention was focused on La^{3+} because its occupation preference in the LaCr-NTO system is not fully understood, and thus has been debatable.[9,10] Due to these reasons, the Cr *K*-edge was not examined. Besides, the Cr *K*-edge (5.99 keV) is also located very close to the La *L*-edge (L_2: 5.89 keV, L_3: 6.27 keV). Thus, the EXAFS spectrum of the Cr *K*-edge was hardly isolated from those of the La *L*-edges. Figure 9 shows the EXAFS spectra at the La *K*-edge for all the doubly doped $NaTaO_3$ and two reference compounds: La_2O_3 and $LaCrO_3$. While the signal-to-noise ratio increased with the increase in the dopant concentration, the shape of the EXAFS oscillations was comparatively similar (Figure 9a). This was a quick hint that the local structure around La^{3+} was insensitive to the dopant concentration.

When we closely inspected the EXAFS oscillation of LaCr-NTO (20+20 mol%), its overall feature was seen to be far more similar to that of $LaCrO_3$ than that of La_2O_3. In addition, when the EXAFS oscillations were Fourier transformed, the radial distribution function of LaCr-NTO (20+20 mol%) was found to be much closer to that of $LaCrO_3$ (Figure 9b). All these results provide evidences that La^{3+} was coordinated to twelve O anions forming LaO_{12} cuboctahedron rather than octahedrally coordinated to six O anions, and therefore allow us to confirm the presence of $LaCrO_3$ solved in the host $NaTaO_3$. In other words, La^{3+}, and thus Cr^{3+}, have sat in the Na site and the Ta site, respectively. Here, we put our attention primarily on LaCr-NTO (20+20 mol%) because among the examined samples, it has the highest dopant concentration, and hence the best signal-to-noise ratio.

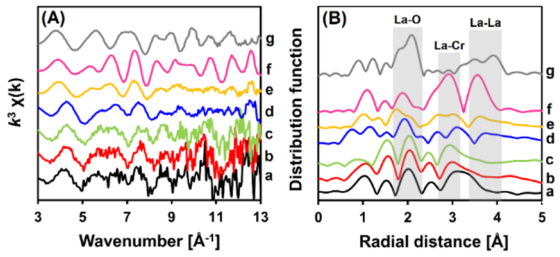

Figure 9. EXAFS spectra at the La *K*-edge of a: LaCr-NTO (1+1 mol%), b: LaCr-NTO (2+2 mol%), c: LaCr-NTO (4+4 mol%), d: LaCr-NTO (8+8 mol%), e: LaCr-NTO (20+20 mol%), f: $LaCrO_3$, and g: La_2O_3. (A) k^3-weighted EXAFS oscillations and (B) radial distribution functions.

In order to test our proposed assignments on the local environment around the absorbing La^{3+}, curve-fitting was performed on the selected data. EXAFS oscillations were first extracted and then Fourier-transformed using the Hanning window with a k^3-weighting and a d*k* of 2. Single-peak fitting was performed without phase correction, and therefore distances of the Fourier transformed contributions were shifted to about 0.4 Å lower than the real crystallographic distances. Four parameters, namely *L* (average atomic distance from the absorbing atom), CN (coordination number), d*E* (the difference in the threshold energy from the reference), and σ^2 (Debye–Waller factor), were allowed to vary.

Fourier-filtered and best-fit oscillations over the *k* range of 3 to 13 Å^{-1} for LaCr-NTO (20+20 mol%) are shown in Figure 10a. The residuals in the *k* space were remarkably small for all three extracted EXAFS oscillations. The radial distribution function of LaCr-NTO (20+20 mol%) obtained from the best-fit oscillation was comparatively plotted with the original distribution in Figure 10b. Four well-separated peaks appeared. The first peak situated at about 1 Å was likely an artifact since we were unable to satisfactorily perform a curve-fitting on this peak despite appreciable efforts which have been made. Indeed, this first peak seems too short to be assigned to the La-O coordination. Therefore, we assigned the second peak located at about 1.7 Å to be the La-O coordination. Meanwhile, the third peak appeared at about 2.9 Å was assigned to the La-Cr coordination. When we assumed the third peak to be composed of the La-Ta coordination, because Ta^{5+} is much heavier than Cr^{3+} and heavier elements reflect electrons more efficiently, we got a poor fit of oscillation. Thus, the assumed La-Ta coordination for the third peak can be ruled out here. As for the fourth peak which appeared at about 3.7 Å, it was assigned to the La-La coordination. Assuming the fourth peak to be the La-Ta coordination also resulted in an unacceptable closeness of fit and low statistical quality of the fitted parameters.

For references, Fourier-filtered and best-fit oscillations of $LaCrO_3$ and La_2O_3 were also presented in Figure S6 and Figure S7, respectively. It was readily noticed that the overall features of the Fourier-filtered and fitted oscillations as well as the observed and fitted radial distribution functions of LaCr-NTO (20+20 mol%) were much closer to those of $LaCrO_3$ than those of La_2O_3. These results strongly indicated the existence of $LaCrO_3$ solved in $NaTaO_3$, and hence the formation of a $LaCrO_3$–$NaTaO_3$ solid solution. The most marked difference in the radial distribution function between LaCr-NTO (20+20 mol%) and $LaCrO_3$ was the relative magnitude of the second peak. In LaCr-NTO (20+20 mol%), the contribution from the La-O coordination was dominant. Meanwhile, the contribution of the second and third coordination shells was limited, presumably because LaCr-NTO was less ordered than $LaCrO_3$.

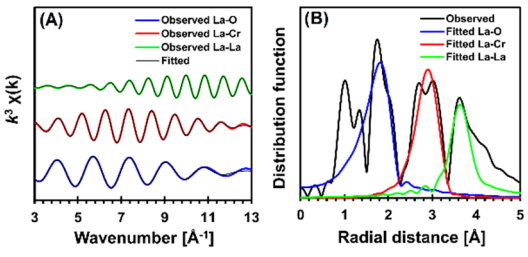

Figure 10. Comparison between observed and fitted EXAFS spectra at the La *K*-edge of LaCr-NTO (20+20 mol%) in (A) *k* space and (B) *R* space.

The results of the curve-fitting for all the observed peaks are summarized in Table 1. We obtained satisfactory goodness of fits; *R*-factors were all lower than 0.02, confirming the reliability of our models adopted for the curve-fitting. Additionally, σ^2 values were also much lower than 0.03 Å^2. If a σ^2 is larger than 0.03 Å^2, the chosen model must be wrong in some way.[20] Here, the important issue to be taken into consideration is the length of the La-O coordination. The length of the La-O coordination in LaCr-NTO (20+20 mol%) was compatible to that in $LaCrO_3$. This was a strong evidence that the absorbing La^{3+} in LaCr-NTO (20+20 mol%) and that in $LaCrO_3$ were of identical species. With this supposition, La^{3+} should have exclusively occupied the Na site, and thus, a $LaCrO_3$-$NaTaO_3$ solid solution should have been formed. As for the La-Cr coordination and the La-La coordination, their lengths in LaCr-NTO (20+20 mol%) were reasonably larger than those in $LaCrO_3$, probably because they were surrounded by $NaTaO_3$ which possesses a larger lattice volume (235.5 Å^3)[16] than $LaCrO_3$ (234.8 Å^3).[15]

Moreover, the other issue to be considered is the coordination number of the La-O shell. In La_2O_3, each La^{3+} was octahedrally coordinated to six O anions. Meanwhile, each La^{3+} in $LaCrO_3$ was coordinated to twelve O anions. The fitted coordination numbers for those two reference compounds (7.3 for La_2O_3 and 12.1 for $LaCrO_3$) were satisfactorily close to the theoretical values. To our surprise, however, the coordination number of the La-O shell in LaCr-NTO (20+20 mol%) was considerably lower than that in $LaCrO_3$ counterpart, presumably due to a less ordered structure of LaCr-NTO.

Table 1 EXAFS curve fitting results.

	Shell	CN	*L* [Å]	d*E* [eV]	σ^2 [Å^2]	*R*-factor
LaCr-NTO	La-O	3.6	2.42	-9.7	0.008	0.013
(20+20 mol%)	La-Cr	2.8	3.43	5.0	0.008	0.018
	La-La	0.6	3.94	9.8	0.003	0.008
$LaCrO_3$	La-O	12.1	2.41	-5.4	0.004	0.010
	La-Cr	6.8	3.38	-4.1	0.008	0.017
	La-La	5.2	3.89	-0.6	0.006	0.002
La_2O_3	La-O	7.3	2.56	-4.0	0.007	0.007
	La-La	4.7	3.99	1.8	0.008	0.014

CN is the coordination number; *L* is the bond length; d*E* is the threshold energy difference; σ^2 is the Debye−Waller factor; *R*-factor is the goodness of fit.

3.7 X-ray photoelectron spectroscopy

The photoelectron spectra of the dopants are presented in Figure 11a. The +3 oxidation state of the La species in the doubly doped NTO was clearly demonstrated. The peaks at the binding energies of 834.5 and 851.1 eV with the shake-up peaks located at 839.1 and 855.8 eV corresponded to the La 3d emissions of 5/2 and 3/2 spin-orbit couplings, respectively. The observed binding energy values were in agreement with the reported value for the La^{3+} in La_2O_3.[21]

Furthermore, the Cr 2p emissions in Figure 11b showed doublet peaks at 576.8 and 586.4 eV, assigned to the 3/2 and 1/2 couplings, respectively. The features of the emissions are characteristic for Cr^{3+} in Cr_2O_3.[10] It is important to note that in all the examined samples, no other peak such as the peak belonging to Cr^{6+} at 580.2 eV [10] was indicated. Creation of Cr species with higher oxidation states did not seem to occur here, possibly because the cationic charge was effectively balanced by La^{3+}. Also, in both La 3d and Cr 2p regions, the spectra of the photocatalyst samples peaked at essentially the same binding energy, indicating that the oxidation state of the dopants was insensitive to the dopant concentration.

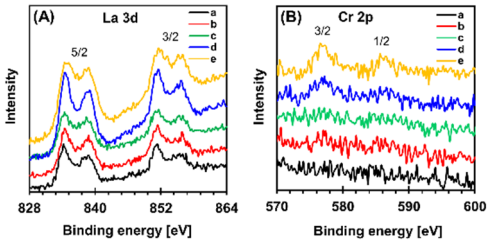

Figure 11. XPS spectra of a: LaCr-NTO (1+1 mol%), b: LaCr-NTO (2+2 mol%), c: LaCr-NTO (4+4 mol%), d: LaCr-NTO (8+8 mol%), and e: LaCr-NTO (20+20 mol%) at (A) La 3d and (B) Cr 2p regions.

3.8 IR absorption induced by photoexcited electrons

Electron population excited by UV light or visible light in the formed solid solution was measured with IR spectroscopy. UV-induced IR has been used for examining the photoactivity of a number of metal oxides.[8,22,23] The light-induced IR absorption indicates a steady population of photoexcited electrons which have not recombined yet with the valence band (VB) holes.[19] The observed IR absorption originates from the intraband transitions of electrons in the CB.

Figure 12a shows the change in the absorption spectra of all the photocatalyst samples under UV light. The absorption spectrum of $LaCrO_3$ was not presented here. The reason is that, despite several attempts which have been made, the CaF_2 plate somehow remained difficult to be entirely covered by the thin film of $LaCrO_3$. The noise of the spectrum was also considerably high owing to the severe light scattering by the highly aggregated $LaCrO_3$ particles. Therefore, the result would not be reliable. While closely examining the obtained absorbance change shown in Figure 12a, continuous increase of IR absorbance was witnessed from 1300 to 900 cm^{-1}. Then, as distinctly noticed here, the absorption of IR light by La-NTO (2 mol%) was far more intense than those by the other photocatalyst samples, indicating a high availability of electrons in the CB. Such a large electron population is one of the reasons for the high efficiency of photocatalytic water splitting with La-NTO (2 mol%) under UV light previously reported.[4] Simultaneously incorporating La^{3+} and Cr^{3+} into NTO also increased the absorbance change, and thus the electron population, to a limited extent.

Here, the significantly increased electron population in La-NTO (2 mol%) was likely due to restricted electron-hole recombination caused by the La^{3+} impurities. The mechanism of restricted electron-hole recombination in La-NTO should be similar to that in Sr-NTO reported earlier.[19,24] On the other hand, in the absence of La^{3+}, Cr^{3+} appeared to promote electron-hole recombination since the integrated absorbance decreased following the Cr^{3+} doping. The exact factor behind the detrimental effect of Cr^{3+} observed here is still unknown, yet likely related to the formation of defects such as oxygen vacancies to balance the cationic charge in the lattice (Eq. 1).

$$Ta^{5+} = Cr^{3+} + O^{2-}\ \text{vacancy} \quad (1)$$

When Cr^{3+} is doped together with La^{3+}, cationic charge balance is achieved without formation of oxygen vacancies (Eq. 2).

$$Na^{+} + Ta^{5+} = Cr^{3+} + La^{3+} \quad (2)$$

Here, La^{3+} contributed to maintaining the cationic charge balance in the solid solution.

IR absorption spectra induced by visible light were also recorded herein since the currently studied LaCr-NTO photocatalysts are intended for visible light photocatalysis. The results are shown in Figure 12b. In this case, NTO and La-NTO (2 mol%) cannot absorb visible light due to their large band gaps. As shown in Figure 12b, IR absorption under visible light was lower than that under UV light despite comparable light irradiance applied. A lower electron population was present in the photocatalyst sample irradiated with visible light. This was not unusual considering the absence of band gap excitation under visible light. Furthermore, under visible light, double doping with La^{3+} and Cr^{3+} was found to be more beneficial than single doping with Cr^{3+} alone in terms of electron population, which was also consistent with the case under UV light. This was suggested to be due to the absence of oxygen vacancies as a consequence of an effective charge balance in the doubly doped NTO. Overall, we here succeeded in sensitizing NTO to visible light with the scheme of charge compensated dopants employing La^{3+} and Cr^{3+}. Electrons can be photoproduced by visible light with a population comparable to that under UV light.

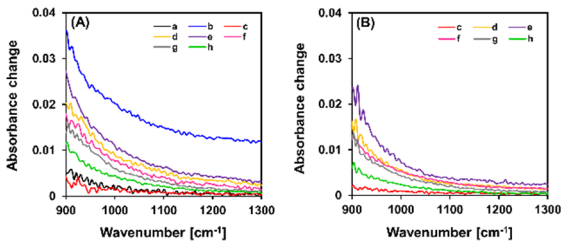

Figure 12. Change in IR absorbance induced by (A) UV light and (B) visible light of a: NTO, b: La-NTO (2 mol%), c: Cr-NTO (2 mol%), d: LaCr-NTO (1+1 mol%), e: LaCr-NTO (2+2 mol%), f: LaCr-NTO (4+4 mol%), g: LaCr-NTO (8+8 mol%), and h: LaCr-NTO (20+20 mol%).

3.9 Origin of enhanced electron population

Now, we come to an important question: what are the origins of the enhanced electron population after double doping of NTO with La^{3+} and Cr^{3+}? We here proposed several plausible factors behind the enhanced electron population. Based on the DR spectra shown in Figure 7, the formation of a partially occupied state within the band gap; hereinafter referred to as mid-gap state, located above the VB edge top was indicated following the double doping. We can observe absorption tail just after the absorption edge. Such absorption tail should be related to the presence of a mid-gap state, which was partially occupied. The partially occupied mid-gap states should enable electron excitations to the CB, and at the same time, receive electrons photoexcited from the VB under either UV light or visible light.

As illustrated in Figure 13, we propose four scenarios of electron excitation. Figure 13a shows the scenario for pristine NTO irradiated by UV light. In this scenario, electrons are excited from the VB to the CB (path 1), referred to as band gap excitation. The photoexcited electrons in the CB absorbed IR light irradiated during the light-induced IR measurement, and the electron population was then quantified. On the other hand, visible light is energetically unable to promote band gap excitation (Figure 13b). No electron is thus

available in the CB to be quantified. After double doping with La^{3+} and Cr^{3+}, a partially filled mid-gap state is formed by Cr^{3+} (Figure 13c). Upon UV light irradiation, electrons in the mid-gap states are excited to the CB (path 2). This electron excitation takes place in parallel with the band gap excitation (path 1). In addition to those two processes, a two-step electron excitation from the VB to the CB via the mid-gap state (path 3) is also energetically allowed to proceed. Although this type of band gap excitation may be insignificant, it remains beneficial to increase the electron population in the CB. Meanwhile, under visible light irradiation, only path 2 and path 3 are possible to occur, considering the high band gap energy of the host NTO which was estimated from the DR spectra to be about 4 eV (Figure 13d).

Altogether, on the basis of the above-presented discussion, continuously increasing the dopant concentration should lead to an increased electron population in the CB, because more mid-gap states are formed to generate more electrons. However, this was not the case for our system, as shown in Figure 12. The largest population of electrons in the doubly doped NTO photoexcited by either UV or visible light was achieved when 2+2 mol% of dopants was incorporated. There was an optimum concentration of dopants within the examined range of concentration. Higher concentrations of dopants appeared to be unfavorable. Other research groups have also reported that high concentrations of dopant are unfavorable for the water splitting activity of LaCr-NTO under visible light.[10,14] In their reports, a volcano-type photoactivity pattern was always observed. The highest photoactivity was achieved at dopant concentrations of 3+3 mol% and 0.3+0.3 mol% when NTO was doped through solid-state route[10] and hydrothermal route[14], respectively. Their results are in agreement with our observations on electron population. Therefore, it may be reasonable to expect that the photoactivity of LaCr-NTO for water splitting is linearly correlated with electron population when assuming that all the photogenerated electrons are usable for reducing protons. In water splitting reaction with LaCr-NTO,[9,10,14] the detrimental effect of dopant at relatively high concentrations was thought to be due to the existence of Cr^{6+}. However, this was not observed in our case. In all the doubly doped samples, only Cr^{3+} was formed according to the XPS results. So, regarding the detrimental effect of dopant observed here, it may be speculated that a higher concentration of dopants has increased lattice defects in some way that trigger the formation of unoccupied mid-gap states situated just below the CB edge bottom and in turn promote electron-hole recombination. Our speculation certainly needs to be further examined and supported by solid evidences obtained from, for example, DFT calculation.

Finally, one may wonder how to achieve further increase of electron population in our photocatalyst system. Our proposals for this purpose would be (1) suppressing the formation of unoccupied states which may act as recombination centers and (2) producing concentration gradient of dopants which can promote an effective charge carrier separation, as was observed previously in our NTO samples singly doped with Sr^{2+}.[19,24-26] Here, the latter proposal may be realized by optimizing the preparation parameters, such as Na/Ta molar ratio, calcination temperature, and calcination time, to kinetically control the formation of doped NTO particles. How to effectively tune the concentration gradient of dopants is an interesting research question for future studies.

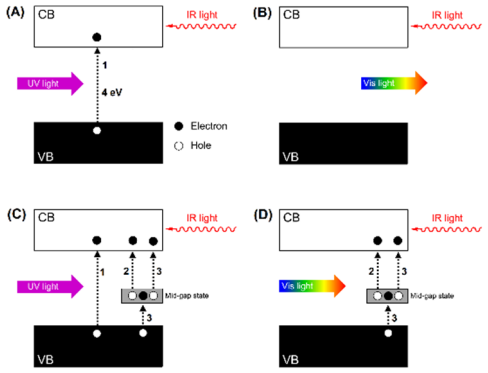

Figure 13. Schematic representation of electron excitation in (A) NTO under UV light, (B) NTO under visible light, (C) LaCr-NTO under UV light, and (D) LaCr-NTO under visible light. Three different pathways of electron excitation are shown here.

Conclusions

In this research, $NaTaO_3$ was doped with La^{3+} and Cr^{3+} through a solid-state route. Using this preparation route, La^{3+} and Cr^{3+} were well received by $NaTaO_3$ in one-to-one ratio. Substitution of La^{3+} for Na^+, and Cr^{3+} for Ta^{5+}, forming a $LaCrO_3$-$NaTaO_3$ solid solution, is suggested. Following the double doping, the lattice of $NaTaO_3$ initially expanded and then shrank to approach that of $LaCrO_3$. When the dopant concentration was continuously increased, the particle size gradually decreased, yet the particle shape remained almost unaltered. No surface reconstruction was seen, indicating the absence of lattice mismatch. Incorporation of La^{3+} and Cr^{3+} with a proper concentration into $NaTaO_3$ led to an increased population of photoexcited electrons under both UV and visible light. Electron population increased the most when 2+2 mol% of dopants were incorporated into $NaTaO_3$. Extended light absorption caused by Cr^{3+} and elimination of oxygen vacancies due to the presence of La^{3+} together with Cr^{3+} for balancing the cationic charge in $NaTaO_3$ are proposed to be behind the increased electron population.

Conflicts of interest

There are no conflicts to declare.

Acknowledgements

H.S. is an International Research Fellow of the Japan Society for the Promotion of Science (JSPS). This work was financially supported by JSPS KAKENHI (Grant: JP18F18029, JP16H02250, and JP18KK0161). X-ray absorption measurement was carried out under the approval of the Photon Factory Advisory Committee (Proposal: 2016G057). Hidenori Saito of Kanagawa Academy of Science and Technology operated the scanning electron microscope.

References

(1) Zhang, L.; Jaroniec, M. *Applied Surface Science* **2018**, *430*, 2.

(2) Ismail, A. A.; Bahnemann, D. W. *Solar Energy Materials and Solar Cells* **2014**, *128*, 85.

(3) Hisatomi, T.; Kubota, J.; Domen, K. *Chemical Society Reviews* **2014**, *43*, 7520.

(4) Kato, H.; Asakura, K.; Kudo, A. *Journal of the American Chemical Society* **2003**, *125*, 3082.

(5) Kudo, A.; Kato, H. *Chemical Physics Letters* **2000**, *331*, 373.

(6) Shimura, K.; Kato, S.; Yoshida, T.; Itoh, H.; Hattori, T.; Yoshida, H. *The Journal of Physical Chemistry C* **2010**, *114*, 3493.

(7) Gómez-Solís, C.; Ballesteros, J.; Torres-Martínez, L. M.; Juárez-Ramírez, I. *Fuel* **2016**, *166*, 36.

(8) Yamakata, A.; Ishibashi, T.-A.; Kato, H.; Kudo, A.; Onishi, H. *The Journal of Physical Chemistry B* **2003**, *107*, 14383.

(9) Yi, Z.; Ye, J. *Journal of Applied Physics* **2009**, *106*, 074910.

(10) Yang, M.; Huang, X.; Yan, S.; Li, Z.; Yu, T.; Zou, Z. *Materials Chemistry and Physics* **2010**, *121*, 506.

(11) Ravel, B.; Newville, M. *Journal of synchrotron radiation* **2005**, *12*, 537.

(12) Iyer, P.; Smith, A. *Acta Crystallographica* **1967**, *23*, 740.

(13) Hashimoto, T.; Tsuzuki, N.; Kishi, A.; Takagi, K.; Tsuda, K.; Tanaka, M.; Oikawa, K.; Kamiyama, T.; Yoshida, K.; Tagawa, H. *Solid State Ionics* **2000**, *132*, 181.

(14) Kang, H. W.; Lim, S. N.; Park, S. B.; Park, A.-H. A. *International Journal of Hydrogen Energy* **2013**, *38*, 6323.

(15) Corrêa, H.; Paiva-Santos, C.; Setz, L.; Martinez, L.; Mello-Castanho, S.; Orlando, M. *Powder Diffraction* **2008**, *23*, S18.

(16) Kennedy, B. J.; Prodjosantoso, A.; Howard, C. J. *Journal of Physics: Condensed Matter* **1999**, *11*, 6319.

(17) Pena, M.; Fierro, J. *Chemical reviews* **2001**, *101*, 1981.

(18) Teixeira, N. G.; Dias, A.; Moreira, R. L. *Journal of the European Ceramic Society* **2007**, *27*, 3683.

(19) An, L.; Onishi, H. *ACS Catalysis* **2015**, *5*, 3196.

(20) Calvin, S. *XAFS for Everyone*; CRC press, 2013.

(21) Barreca, D.; Gasparotto, A.; Maragno, C.; Tondello, E.; Bontempi, E.; Depero, L. E.; Sada, C. *Chemical Vapor Deposition* **2005**, *11*, 426.

(22) Yamakata, A.; Ishibashi, T.-A.; Onishi, H. *Chemical Physics Letters* **2001**, *333*, 271.

(23) Furuhashi, K.; Jia, Q.; Kudo, A.; Onishi, H. *The Journal of Physical Chemistry C* **2013**, *117*, 19101.

(24) An, L.; Park, Y.; Sohn, Y.; Onishi, H. *The Journal of Physical Chemistry C* **2015**, *119*, 28440.

(25) An, L.; Sasaki, T.; Weidler, P. G.; Wöll, C.; Ichikuni, N.; Onishi, H. *ACS Catalysis* **2018**, *8*, 880.

(26) An, L.; Kitta, M.; Iwase, A.; Kudo, A.; Ichikuni, N.; Onishi, H. *ACS Catalysis* **2018**, *8*, 9334.

Atom-scale structure of $LaCrO_3$-$NaTaO_3$ solid solution photocatalysts with enhanced electron population

Hanggara Sudrajat,[a,*] Yizhong Zhou,[a] Takuro Sasaki,[b] Nobuyuki Ichikuni,[b] Hiroshi Onishi[a]

[a]*Department of Chemistry, Graduate School of Science, Kobe University, Kobe 657-8501, Japan*

[b]*Department of Applied Chemistry and Biotechnology, Graduate School of Engineering, Chiba University, Chiba 263-8522, Japan*

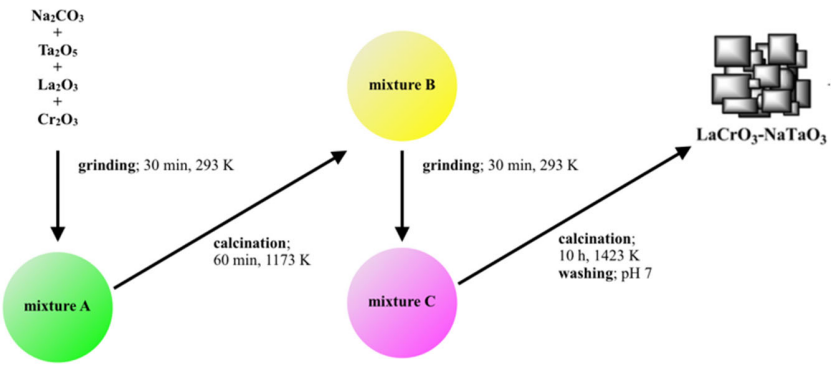

Figure S1. Illustration of the preparation of LaCr-NTO through the solid-state route.

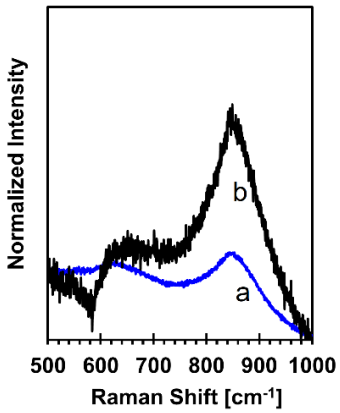

Figure S2. Raman spectra of a: LaCr-NTO (50+50 mol%) and b: LaCr-NTO (75+75 mol%).

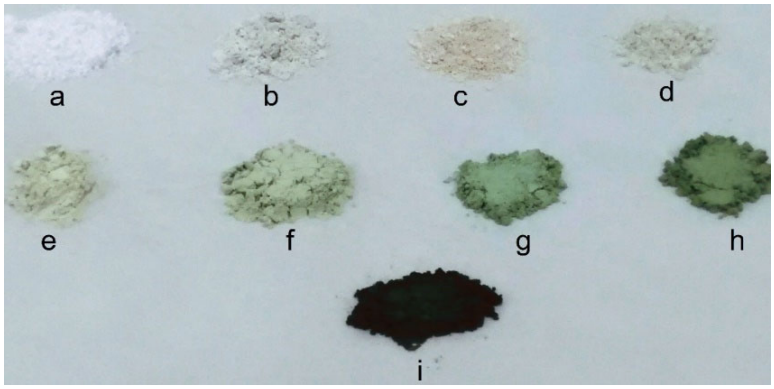

Figure S3. Photographs of a: NTO, b: LaCr-NTO (1+1 mol%), c: LaCr-NTO (2+2 mol%), d: LaCr-NTO (4+4 mol%), e: LaCr-NTO (8+8 mol%), f: LaCr-NTO (20+20 mol%), g: LaCr-NTO (50+50 mol%), h: LaCr-NTO (75+75 mol%), and i: $LaCrO_3$

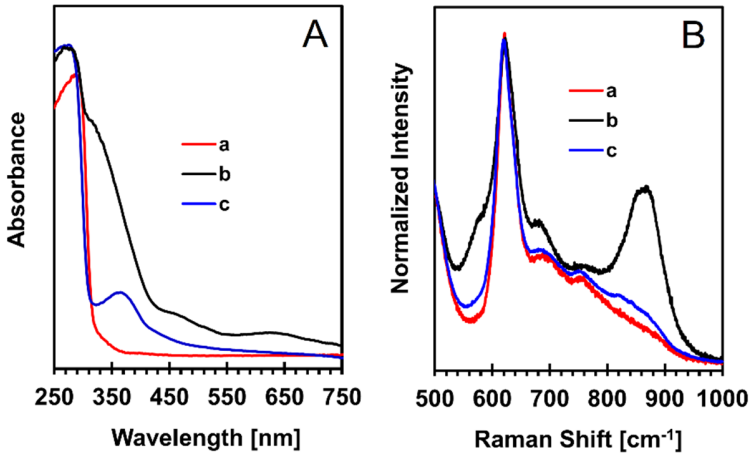

Figure S4. (A) DR spectra and (B) Raman spectra of a: NTO, b: LaCr-NTO (4+4 mol%), and c: the physical mixture of 50 wt% La-NTO (4 mol%) and 50 wt% Cr-NTO (4 mol%).

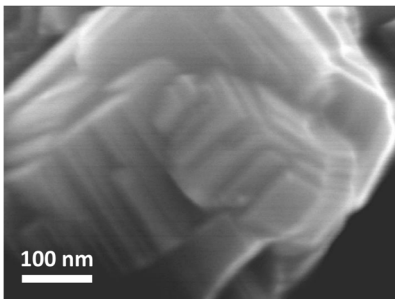

Figure S5. SEM image of La-NTO (2 mol%).

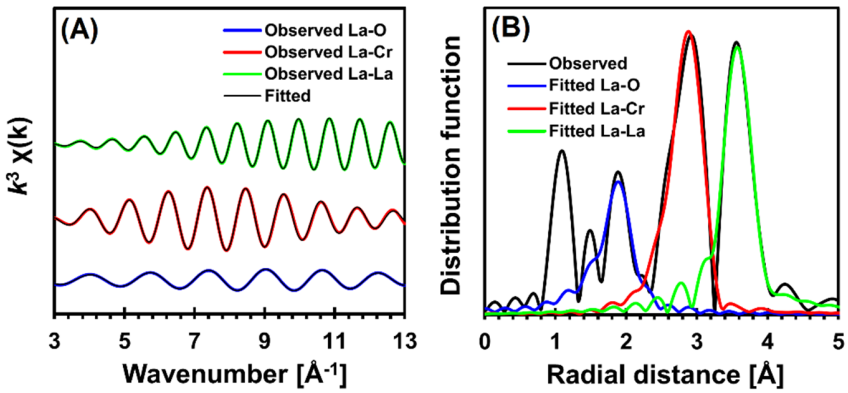

Figure S6. Comparison between observed and fitted EXAFS spectra at the La *K*-edge of $LaCrO_3$ in (A) *k* space and (B) *R* space.

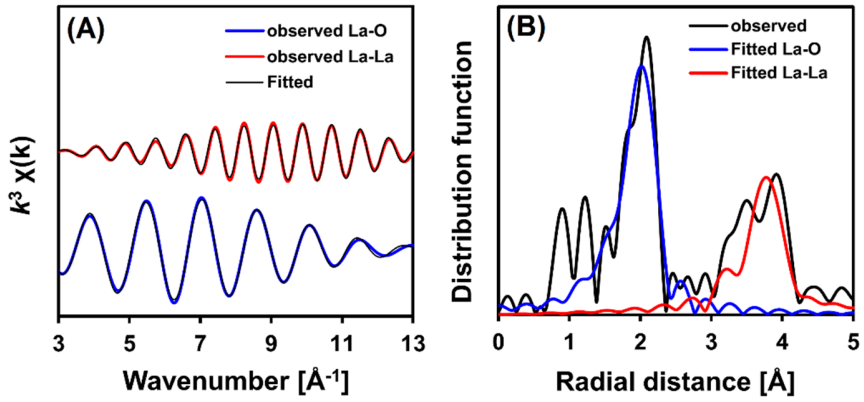

Figure S7. Comparison between observed and fitted EXAFS spectra at the La *K*-edge of La_2O_3 in (A) *k* space and (B) *R* space.